International Journal of Intelligent Information and Management Science
ISSN: 2307-0692, Volume 6, Issue 5, October, 2017

Surface Design based on Geometric Flow Method and Tessellation

Shuaili Wang
Hunan City University, Yiyang, 413000, China

Abstract: This paper combines geometric flow method with tessellation and make full use of their respective strengths to complete some surface design problems, such as surface blending, N sides fill holes and others which satisfy G1 boundary conditions. Based on full analysis of subdivision, the technology utilizes the discrete of four-order geometric flows to successfully construct four-order geometric partial differential equations' finite element method based on quadrilateral surface subdivision. Experimental results show that: surface design which based on geometric flow method and surface subdivision is effective and correct.

Keywords: Discrete; Surface Blending; Geometric Partial Differential Equations; Diffusion Flow

1. Introduction

Surface design has been formed a theoretical system which takes NURBS parametric feature technology and implicit algebraic surfaces as the main body, takes interpolations, fitting, approaching as the skeleton. As computer graphics requirements for the authenticity of objects increase, the object's geometric design complexity increases and research areas the expands, using only parametric polynomial has been far from able to satisfy demand, it is urgent to call for new ways to solve new problems that appear in various research areas. So segmentation techniques, partial differential equations methods have been widely applied to these emerging field of study [4].

Subdivision method

As shown in Figure 3, for vertexes $q_0^{(l)}$ with degree on l (l = 0,1,2, ...) subdivision level , supposed that directly adjacent vertexes in the mesh is $q_0^{(l)}$, $q_1^{(l)}$, $q_2^{(l)}$, $q_n^{(l)}$, then new location $q_0^{(l+1)}$ of the vertex $q_0^{(l)}$ on $l+n$ level and directly adjacent vertexes $q_i^{(l+1)}\,(i=1,...,n)$ can be obtained by using the following vertex-point / side point rules.

$$q_0^{(l+1)} = \frac{w_0(n)q_0^{(l)} + q_1^{(l)} + q_2^{(l)} + \mathbf{L} + q_n^{(l)}}{w_0(n)+n} \tag{1}$$

Template edge point,

$$q_i^{(l+1)} = \frac{3q_0^{(l)} + 3q_i^{(l)} + q_{i-1}^{(l)} + \mathbf{L} + q_{i+1}^{(l)}}{6} \tag{2}$$

foot code of the two formulas take n as the model.

$$\begin{aligned} w_0(n) &= n / a(n) - n \\ a(n) &= \frac{5}{8} - \left[3 + 2\cos(2p/n)\right]^2 / 128 \end{aligned} \tag{3}$$

Use the above rules to conduct subdivision iteration on triangular mesh and control grid, then a smooth limit surface will be converged. Each vertex v of initial control mesh can find a corresponding point $v\infty$ on the limit surface . *M.uller* etc put forward the formula to strike $v\infty$ and its two non-collinear cut vectors u_1 and u_2 on limit surface, then normal direction of surface at $v\infty$ point can be obtained .

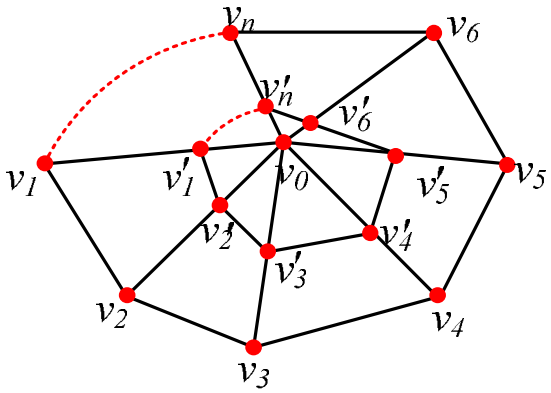

Figure 1. Generation of triangular mesh point and its adjacent vertexes on l+1 subdivision hierarchy

Boundary treatment, edit and modification of curves are as follows:

Conduct respectively once and twice subdivision o the initial grid. It is not difficult to find that the subdivided grid is also dense in where the initial control triangle network is dense; relatively straight edges of control network on plowshare site become jagged after subdivision ; The outer edge of the wing plow and the edge of plows chest are not smooth, which are not expected. Its main causes are that subdivision rules are used for ver-

tex-point and edge point on the border of the grid and inside the grid during subdivision.

In order to eliminate the affect of subdivision process on the geometric properties of control mesh boundary, it is necessary to modify the generation rules for the vertex point and edge point of boundaries.

It is needed to respectively treat borders that maintain smooth and straight, mark respectively the initial mesh vertexes .For the former, the boundary vertex point just needs to remain unchanged, and the boundary edge point only needs to do linear interpolation on the end points of the edge; The latter, in order to make the surface smooth at the boundary point, it needs to modify the weight of the vertex point and edge point template which take the boundary points as end points and the inner side edge point template, the modified rules are shown in Figure 2.Among which,

$$k_1 = 1/4 \quad k_2 = 1/2$$

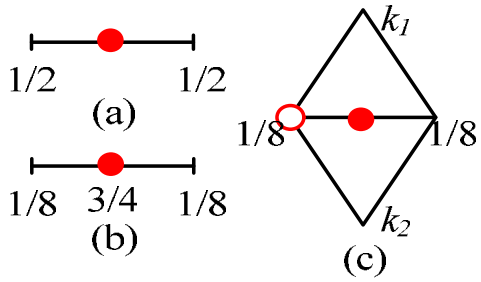

Figure 2. Templates of vertex points and edge points in modified grid boundary vertex

More generally, the boundary control method is to introduce a normal into the grid. Normal control can achieve an arbitrary boundary surface control by changing the size of the right of boundary points' subdivision rule, and through the subdivision process control mesh can be generated from the original breakdown of the various resolution mesh model. These grid models can be used as input of finite element calculation or dynamic simulation software, through the establishment of soil plow surface movement along mattress mechanical model. By conducting finite element calculation or simulation on the plow surface under different tillage speeds, tillage depth, soil deformation and soil condition mattress and other conditions of work performance and efficiency, the basis for the design of complex plow surface can be provided.

2. Equation Model and Its Weak Form

Equation models of surface diffusion flow, Will more flow and surface diffusion flow are listed below. Let S be a closed orientable surface of R_3 it is needed to find a family of smooth and orientable surface set $\{s(t): t \geq 0\}$, which meet below conditions:

$$\begin{cases} \dfrac{\partial x}{\partial t} = -2\Delta_s Hn, \ S(0) = S_0 \\ \partial S(t) = \Gamma \end{cases} \tag{4}$$

Among which, Δs represents the Laplace-Beltrami operator defined on surface s, R and n respectively denote the mean curvature and surface normal vector of the surface. Surface diffusion flow has the nature to reduce the volume and size.

$$\begin{cases} \dfrac{\partial x}{\partial t} = -\left[\Delta_S R + 2R(R^2 - K)\right]n, \ S(0) = S_0 \\ \partial S(t) = h \end{cases} \tag{5}$$

Wherein, in addition to defined operator in formula (1) , K represents the Gaussian curvature on the surface S. Surface which satisfies the equation $\Delta_S R + 2R(R^2 - K) = 0$ is called Will more surface or sheet surface, it occurs as a critical point of functional area.

$$W(S) := \int_S R^2 ds \tag{6}$$

3. Discrete of Four Order Geometric Flows

Equation's finite element discretization will be described as below. First, introduce two finite element space $E_r = span[\Omega_1, \Omega_2, ...\Omega_n]$ and $F_r = span[\Omega_1, \Omega_2, ...\Omega_n]$. In E_r and F_r, carry out spatial discrete for the control vertex x, mean curvature H and mean curvature normal R. Let T be a quadrilateral control mesh of surface s, its control vertex is denoted as $\{x_j\}_{i=1}^{n}$. Classification of the control vertexes is provided in the following. The first category are interior vertexes , whose location are unknown and they are the amount to be solved in this paper , denoted as $\{x_j\}_{i=1}^{n_0}$.For curved stitching or N-sided hole filling problem, it requires internal vertexes in stitching or patching area. The rest of the control vertexes are denoted as $\{x_j\}_{i=n_0+1}^{n}$, they are known quantity. Continue to carry on classification. Denote vertex which is adjacent to internal vertex $\{x_j\}_{i=1}^{n_0}$ as $\{x_j\}_{i=n_2+1}^{n_2}$ within two circles. Then the remaining vertexes are denoted as $\{x_j\}_{i=n_2+1}^{n_0}$, the mean curvature of these vertexes is known. So unknowns need to be solved is the position $\{x_j\}_{i=1}^{n_0}$ of the control vertex, mean curvature $\{R_i\}_{i=1}^{n_2}$ and mean curvature vector $\{R_i\}_{i=1}^{n_2}$ can be written as

$$x(t) = \sum_{j=1}^{n_0} f_j x_j(t) + \sum_{j=n_0+1}^{n} f_j x_j(t), x_j(t) \in R^3 \tag{7}$$

$$R(t)=\sum_{j=1}^{n_2} j_j R_j(t)+\sum_{j=n_2+1}^{n} j_j R_j(t), R_j(t)\in R \quad (8)$$

$$R(t)=\sum_{j=1}^{n_2} j_j R_j(t)+\sum_{j=n_2+1}^{n} j_j R_j(t), R_j(t)\in R^3 \quad (9)$$

Wherein $R_j(t)$ and $R(t)$ respectively represents the mean curvature and the mean curvature vector at the vertex x_j. In this paper, basis functions Ω_j and h_j of each vertex x_j are all limit function form of Catmull-Clark subdivision format, the value at the control point x_j is 1, the value is 0 at the other points. Branched groups of Ω_j and h_j are local, including the vertexes within 2 circles around control point x_j. In actual calculation, the parameter value is taken as a unit within the quadrilateral Gauss nodes. If vertex x j is non-rule-based, partial subdivision can be carried out in its vicinity until Gauss point parameter values fall into a regular bi-cubic B-spline surface chip.

Put the discretization form formula (7) (8) of control vertex x and mean curvature H in the finite element space into equation (4) (5), taking the trial function $\{\Omega_i\}_{i=1}^{n_0}$ and $\{\Omega_i\}_{i=1}^{n_2}$, by the known condition it can be known that $b\, x_j(t)/b_t=0$ (when j **f** n_0, x_j is fixed). Then put the items which are relative to the known control vertex $\{x_i\}_{i=n_0+1}^{n}$ and the mean curvature $\{R_i\}_{i=n_2+1}^{n}$ to the right side of equation, then get matrix form of formula (4) (5) as the following

$$\begin{cases} M_{n_0}^{(1)}\dfrac{\partial X_{n_0}(t)}{\partial t}+L_{n_2}^{(1)}Y_{n_2}(t)=B^{(1)} \\ M_{n_2}^{(2)}Y_{n_2}(t)+L_{n_0}^{(2)}X_{n_0}(t)=B^{(2)} \end{cases} \quad (10)$$

The elements of which are defined as follows:

$$m_{ij}^{(1)}=[\int_s f_i f_j dA]I_3, m_{ij}^{(2)}=\int_s j_i j_j dA;$$

$$l_{ij}^{(1)}=\begin{cases} 2\int_s [f_i \varnothing j_j - n(\nabla s j_j)^T \nabla s j_j]dA, \text{ for SDF} \\ \int_s [f_i[\varnothing j_j + 2n(H^2-K)j_j]-n(\nabla s f_i)^T \nabla s j_j]dA, \text{ for WF} \end{cases}$$

$$l_{ij}^{(2)}=-\frac{1}{2}\int_s [j_i(\varnothing f_j)^T-(\nabla s j_i)^T \nabla s f_j n^T]dA \quad (11)$$

The dimension of the right hand side are $C(1)\in R_3 n_0$, $C(2)\in Rn_2$.

Similarly, put equation (10) (11) into equation (12), similarly, matrix form of formula (12) is as

$$\begin{cases} M_{n_0}^{(3)}\dfrac{\partial X_{n_0}(t)}{\partial t}+L_{n_2}^{(3)}Y_{n_2}(t)=C^{(3)} \\ M_{n_2}^{(4)}Y_{n_2}(t)+L_{n_0}^{(4)}X_{n_0}(t)=C^{(4)} \end{cases} \quad (12)$$

The elements of which are defined as follows:

$$m_{ij}^{(3)}=\int_s f_i f_j dA, m_{ij}^{(4)}=\int_s j_i j_j dA;$$

$$l_{ij}^{(3)}=-2\int_s (\nabla s j_j)^T \nabla s f_i dA, \quad (13)$$

$$l_{ij}^{(4)}=\frac{1}{2}\int_s (\nabla s f_j)^T \nabla s j_i dA.$$

The dimension of the right hand side are $C(3)\in Rn_0\times 3$, $C(4)\in Rn_2\times 3$.

In the following conduct time discretization. For formula (14), assuming there areapproximate solution $x_{n_0}^{(k)}=x_{n_0}(t_k)$ and $x_{n_2}^{(k)}=x_{n_2}(t_k)$ when time $t=t_k$. Semi-implicit Euler scheme can be used to construct the approximate solution $x_{n_0}^{(k+1)}=x_{n_0}(t_k+1)$ and $x_{n_2}^{(k+1)}=x_{n_2}(t_k+1)$ when $t=t_{k+1}=t_k+t(k)$, namely use $[x_{n_0}(t_{k+1})-x_{n_0}(t_k)]/t^{(k)}$ to replace the derivative $\partial X_{n_0}(t)/\partial t$, surface data when $t=t_k$ is used to calculate matrix $M(1)$, $M(2)$, $L(1)$ and $L(2)$ of formula (14).

Then result in a linear system for solving $x_{n_0}^{(k+1)}$ and $x_{n_2}^{(k+1)}$.

$$\begin{bmatrix} M_{n_0}^{(1)} & t^{(k)}L_{n_2}^{(1)} \\ L_{n_0}^{(2)} & M_{n_2}^{(2)} \end{bmatrix}\begin{bmatrix} X_{n_0}^{(k+1)} \\ Y_{n_2}^{(k+1)} \end{bmatrix}=\begin{bmatrix} t^{(k)}B^{(1)}+M_{n_0}^{(1)}X_{n_0}^{(k)} \\ B^{(2)} \end{bmatrix} \quad (14)$$

Noted that although $M(1)$ and $M(2)$ of the coefficient matrix is symmetric positive definite, but the overall coefficient matrix is not symmetric positive definite. In this paper, the GMRES iterative method proposed by s a a_d is used to solve the system.

4. Simulation and Analysis

If the area to be filled is small, the evolution difference is very small. Compared to the first row in Figure 5, there is no significant blending surface difference of the three four order streams in the second row.

4.1. Side fill holes

Given surface mesh with holes, it is needy to construct the surface patches with G_1 smooth on boundary. Figure 7 shows an frog model of N-sided hole filling. Figure 7c shows the restored surfaces after 2 iterations by using WF, the time step length is 0.00001. SDF and QSDF's evolution results are similar.

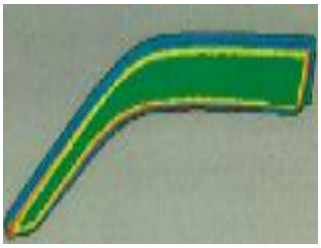

(a)

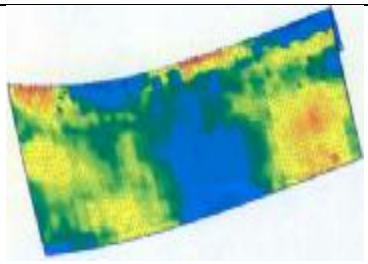

(b)

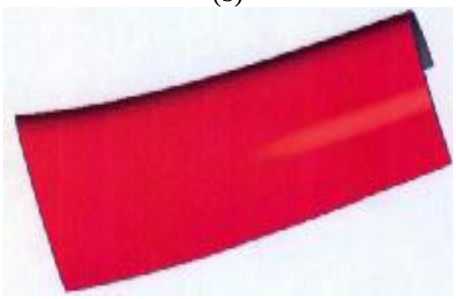

(c)

Figure 3. Frog model with N side filling hole

4.2. Examples Verification

Example 1: Given the control point matrix $matrix\left(p_{ij}\right)^{2\times 2}$ of the surface:

$$\begin{bmatrix} (-1,-1,0) & (-1,0,1) & (-1,1,0) \\ (0,-1,1) & \text{Unknown} & (0,1,1) \\ (1,-1,0) & (1,0,1) & (1,1,0) \end{bmatrix}$$

At this point, $i=k=h=n=m=4$, B-spline surface is a pair of quadric surfaces with 33 control vertexes . Wherein, the required internal control point is just a p_{20}, so that equation (1) contains only one formula. By the program it can be calculated that the unknown internal control vertexes are $p_{20}=(0,0,0.6)$, so that the required uniform surface can be drawn out , as shown in Figure 8. The surface area is 4.213, the maximum absolute value of mean curvature surface is 1.701 and the average value is 0.791.

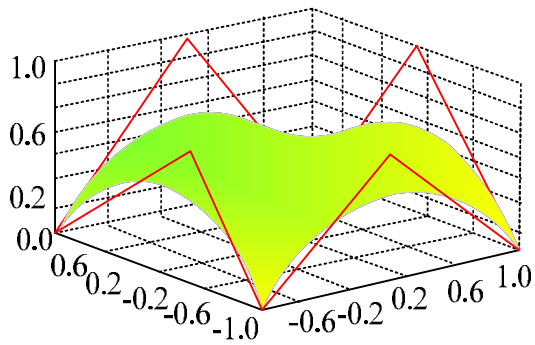

Figure 4. Surface that contains only one internal control vertex

Example 2: Given the control point matrix $matrix\left(p_{ij}\right)^{3\times 3}$ of the desired surface:

$$\begin{bmatrix} (-1,-1,0) & (-1,-0.5,0.5) & (-1,0.5,0.5) & (-1,1,0) \\ (-0.5,-1,0.5) & \text{Unknown} & \text{Unknown} & (-0.5,1,0.5) \\ (0.5,-1,0.5) & \text{Unknown} & \text{Unknown} & (0.5,1,0.5) \\ (1,-1,0) & (1,-0.5,0.5) & (1,0.5,0.5) & (1,1,0) \end{bmatrix}$$

Use bi-quadratic uniform B-spline surfaces to design, i,e , $i=h=4$, $n=m=4$, the number of control vertexes is 44. Among them, there are four required internal control vertexes, so the formula (15) contains four equations, we can calculate the four internal control vertexes:

$$\begin{aligned} &P_{22}=(-0.5,-0.5,0.375),P_{23}=(-0.5,0.5,0.375), \\ &P_{32}=(0.5,-0.5,0.375),P_{33}=(0.5,0.5,0.375). \end{aligned} \tag{15}$$

The obtained B-spline minimal surfaces are shown in Figure 9. The surface area is 4.125, the maximum absolute value of mean curvature surfaces is 6 and the average value is 1.413.

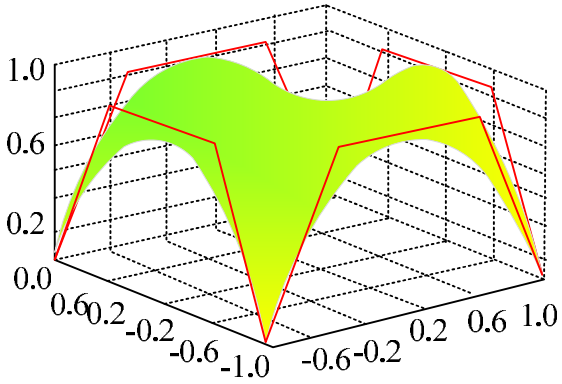

Figure 5. Surface that contains four internal control vertexes

5. Conclusion

This article organically combines the two together and give full play to the advantages of both, in a unified framework it solves some surface design problems such as surface blending, N side fill holes and others which meet G_1 boundary conditions. This paper has successfully constructed the finite element method for surfaces of four order geometric partial differential equations based on quadrilateral Catmull-Clark subdivision.

References

[1] Juan C. Minano, Pablo Benitez, Wang Lin, Jose Infante, Fernando Munoz and Asuncion Santamaria, An application of the SMS method for imaging designs, OPTICS EXPRESS 17(26): 24036-24044, 2009.

[2] Fabian Duerr, Pablo Benitez,Juan C. Minano,Youri Meuretand Hugo Thienpont, Analytic design method for optimal imaging: coupling three ray sets using two free-form lens profiles, OPTICS EXPRESS 20(5): 5576-5585, 2012.

[3] Jia Hou, Haifeng Li, Zhenrong Zheng,Xu Liu. Distortion Correction for Imaging on Non-planar Surface Using Freeform Lens, Optics Communications 285(6): 986-991, 2012.

[4] Dewen Cheng, Yongtian Wang, Hong Hua, M. M. Talha, Design of an optica see-through head-mounted display with a low f-number and large field of view using a freeform prism, APPLIED OPTICS, Vol.48(]4): 2655-2668, 2009.

[5] John Bortz, Narkis Shatz and David Pitou, Optimal design of a nonimaging projection lens for use with an LED source and a rectangular target, Proc. of SPIE, 4092: 130-138, 2000.